J. Fluid Mech. (1995), *vol.* 286, *pp.* 1–23

Interaction of surface waves with turbulence: direct numerical simulations of turbulent open-channel flow

By VADIM BORUE[1], STEVEN A. ORSZAG[1] AND ILYA STAROSELSKY[2]

[1] Applied and Computational Mathematics, Princeton University, Princeton, NJ 08544, USA

[2] Cambridge Hydrodynamics, Inc., PO Box 1403, Princeton, NJ 08542, USA

(Received 8 January 1993 and in revised form 19 September 1994)

We report direct numerical simulations of incompressible unsteady open-channel flow. Two mechanisms of turbulence production are considered: shear at the bottom and externally imposed stress at the free surface. We concentrate upon the effects of mutual interaction of small-amplitude gravity waves with in-depth turbulence and statistical properties of the near-free-surface region. Extensions of our approach can be used to study turbulent mixing in the upper ocean and wind–sea interaction, and to provide diagnostics of bulk turbulence.

1. Introduction

Free-surface turbulent flows are important in physical oceanography, atmospheric science, civil engineering, and industrial technology. From the point of view of fundamental research, free-surface turbulence is a problem which bridges surface wave phenomena and fully developed hydrodynamic turbulence. Also, the theory of surface waves has played a central role in nonlinear science and has been a source of many seminal analytical and computational ideas. Usually, studies of surface wave phenomena have concentrated on the behaviour of non-dissipative, although highly dispersive and nonlinear, ensembles of waves. In this case, potential flow is a good approximation since molecular viscosity is important only within a thin boundary layer $l_v \approx 2\pi(\nu^2/g)^{1/3}$ which is normally smaller than all the characteristic scales such as the capillary length or system dimensions. It is usually assumed that, inside this viscous layer, large vorticity is generated. These vortex sheets move with the surface but play a rather minor role in the large-scale surface dynamics. Their role, however, may be important in small-scale ocean–air interaction, e.g. short gravity waves, capillary waves and wind-generated ripples. At the same time, dissipation and vorticity generation phenomena are essential within the turbulent fluid.

In this paper, we shall concentrate upon the effects of the mutual influence of random surface waves and statistical properties of the near free-surface region in fully developed turbulent flow. To date, there is no comprehensive strong coupling theory of these phenomena. The method used here is that of direct numerical simulation (DNS). The success of early moderate Reynolds number DNS experiments for channel flows with rigid walls encourages the present study of open-channel flow with gravity waves on the surface.

At the present time, rather extensive experimental studies of turbulent open channels exist (Ueda *et al.* 1977; Nezu & Rodi 1986; Kirkgoz 1989), as well as semi-empirical

theories and results of K–$\mathscr{E}$ and Reynolds stress modelling (Gibson & Rodi 1989; Celik & Rodi 1984; Swean *et al.* 1991). The advantage of the DNS approach taken here is its independence of any of the *ad hoc* assumptions often necessary for theory to progress and its greater flexibility in matching experimental conditions. The disadvantages of DNS, at least with our current approach, are mostly related to the fact that we are restricted to consideration of very small-amplitude surface waves, not to mention the usual restrictions on Reynolds number. In fact, as will become clear later, we can consider only wave heights which are smaller than the boundary layer thickness l_v, and in this sense, the waves are 'infinitesimally' small. However, we believe that it is important to develop a DNS technique which handles these open surface flow phenomena. Possible modifications of our approach could extend its applicability range and achieve a level of description of practically important flows. Here we will concentrate on the fundamental, and unfortunately not so practical, aspects of the problem. As a natural first step we start our studies with channel flow bounded by a rigid wall from below and having an open upper surface. Some DNS calculations of open-channel flow have already been performed by Handler *et al.* (1991), Leighton *et al.* (1991) and Swean *et al.* (1991). However, in those early works only the case of zero Froude number was considered. The numerical scheme used in our simulations coincides in the case of zero Froude number with that of Swean *et al.* (1991). In our work we mostly concentrate on the study of spectral properties of the near-free-surface region for non-zero Froude number.

This paper is organized as follows. In §2, we formulate our approach to the problem and then in §3 describe the numerical scheme. In §4, we present the results of simulations of flows with two different mechanisms of turbulence production: shear at the bottom and externally imposed stress at the free surface. In §5, we discuss the applications of our results to problems of physical oceanography, as well as possible extensions of our approach.

2. Open channel with random waves at the surface

We solve the three-dimensional Navier–Stokes equation for incompressible flow:

$$\left.\begin{aligned} \partial_t v_i &= [\boldsymbol{v}\times\boldsymbol{\omega}]_i - \nabla_i \pi + \nu \Delta v_i, \\ \partial v_i/\partial x_i &= 0, \end{aligned}\right\} \tag{1}$$

where $\boldsymbol{v}$ is the velocity field, p is the pressure, $\pi = p/\rho + \frac{1}{2}v^2$, ν is the kinematic viscosity and ρ is the density of fluid. The boundary conditions are

$$\left.\begin{aligned} v_i|_{rigid\ wall} &= 0, \\ n_i \tau_{ij}|_{free\ surface} &= n_i \tau_{ij}|_{ext}, \end{aligned}\right\} \tag{2}$$

where $\tau_{ij} = p\delta_{ij} + \nu\rho(\partial_i v_j + \partial_j v_i)$ are the internal and external components of the stress tensor respective to the fluid, and n_i is the normal to the free surface (and summation over repeated indices is implied). The system (1), (2) is closed using the equation for the free-surface height h:

$$\partial_t h + v_\alpha \partial_\alpha h = v_{normal}|_{fs}. \tag{3}$$

Here an index denoted by the Greek letter α corresponds to a direction in the free surface (the x, y-plane) and ∂_α stands for the differentiation in that direction. The rigid wall is located at $z = -\frac{1}{2}H$, the upper boundary of the physical domain is given by $z = \frac{1}{2}H + h(x, y, t)$, and the subscript fs designates values taken at the free surface.

DNS of fully developed turbulent flows in channels is usually performed using high-resolution spectral methods. To calculate a flow bounded between two rigid walls, the

flow is reproduced by a Fourier spectral series in the x, y-direction and by a Chebyshev polynomial representation in the z-direction. The latter concentrates collocation points towards the walls, providing high resolution of boundary layers. However, in an open channel the upper surface is curved and time dependent, which complicates the use of spectral methods. One possible approach is to give up the high resolution in the z-direction provided by using the Chebyshev polynomials. However, we believe that it is essential to ensure proper resolution of near-free-surface boundary layers, especially in the case where the turbulence is generated by an oscillating stress imposed at the free surface.

The approach used here is based upon linearization of the boundary conditions at the free surface. Then the boundary conditions (2) are adjusted to those imposed at the unperturbed surface $z = \frac{1}{2}H$. Obviously, the ability to describe effects of nonlinear self-interactions of surface waves is sacrificed. On the other hand, such an approach retains the ability to use the Chebyshev spectral method in the z-direction to achieve high resolution. The boundary conditions then take the form

$$\left.\begin{aligned} \partial_t h + \partial_\alpha (h v_\alpha) &= v_z, \\ \rho\nu(\partial_\alpha v_z + \partial_z v_\alpha) &= \tau_{\alpha z}|_{ext}, \\ gh - \sigma_* \Delta h + 2\nu \partial_z v_z &= (p/\rho) - p_{ext}/\rho, \end{aligned}\right\} \tag{4}$$

where g is the gravitational constant, $\sigma_* = (\sigma/\rho)$ is the surface tension, $\tau_{\alpha z}|_{ext}$ and p_{ext} are the external stress and pressure, respectively. All terms in (4) are evaluated at $h(x, y, t) = 0$; again the index α means that only horizontal components are used. The only nonlinear term retained in (4) is the term $\partial_\alpha(hv_\alpha)$ responsible for the convection of the free surface by the horizontal velocity. It turns out that in our formulation the convective term is of the same order of magnitude as v_z though $\partial_\alpha h$ is small. Equations (1) and (4) represent the final formulation of the boundary problem that we use here to describe open-channel flow. In linear approximation, this system reproduces both the dispersion relation of surface waves and the Helmholtz instability at the surface. Interaction effects are accounted for by the nonlinearity of the Navier–Stokes equation.

What are the applicability limits of our approach? First, a linear analysis (Landau & Lifshitz 1987) shows that, for each spatial harmonic with a wavenumber k and the amplitude h, linear approximation of the boundary conditions is only valid when $h \leqslant l_w$, where $l_w = (2\nu/\Omega(k))^{1/2}$ and $\Omega(k) = (gk + \sigma_* k^3)^{1/2}$. It will be seen later that the Fourier spectrum of $h(k)$ is rather steep and the condition $kh(k) \leqslant l_w$ is automatically satisfied whenever it is valid at the smallest wavenumbers. This leads to the estimate for the flow 'integral' Froude number (here and later $\sigma_* = 0$ is assumed)

$$F_i = U/(gH)^{1/2} \ll 10/Re^{1/3}. \tag{5}$$

Here this integral Froude number and the Reynolds number $Re = UH/\nu$ are defined using the centreline velocity U and the channel height. Deriving (5) we assumed that $h \approx u_{rms}^2/2g$. We also assumed that in the range of flow Reynolds numbers of interest here, $Re \approx 10^3$–10^4, the characteristic r.m.s. velocity at the surface can be heuristically estimated as $u_{rms} \approx 10^{-1}U$ (Kim, Moin & Moser 1987).

At the same time it would not be satisfactory to consider only waves that are shorter than the viscous sublayer width l_v and whose amplitude is smaller than l_v. The dissipation length of waves l_v is defined as the scale where the frequency of the wave is equal to the wave decay rate (see (17) below). If that were the case, our analysis would only be of general methodological interest and not applicable to the description of real phenomena in water waves. Indeed, in water at normal conditions, $l_v \approx 10^{-2}$ cm,

whereas the capillary length $d = (2\sigma_*/g)^{1/2} = 10^{-1}$ cm. It is clear that any length scales smaller than d are not of interest for engineering and oceanographic applications because they are effectively damped by capillary effects.

The condition for the existence of wave motion is $l_v \leqslant h$, resulting in the inequality

$$F_i \geqslant 10/Re^{1/2}. \tag{6}$$

It is clear that as $Re \to \infty$ there exists a wide range of Froude numbers where both inequalities (5) and (6) hold. It is worth mentioning that in a typical flow of engineering interest ($H \approx 1$ m, $U \approx 0.1$ m s^{-1}, $Re \approx 10^4$, $F_i \approx 10^{-1}$) the condition (5) is satisfied. This is also the case for the typical laboratory setup in the free-surface-flow studies of Ueda *et al.* 1977.

3. Numerical procedure

The numerical procedure used here is similar to that used by Kim *et al.* (1987) for rigid-channel flow. A spectral method, with Fourier series in the streamwise (x) and spanwise (y) directions, and Chebyshev polynomial expansion in the normal direction (z), is employed spatially. A conventional time-splitting scheme is used to separate nonlinear and viscous time steps. However, the solution for incompressibility and viscosity is done within the same step by solving a fourth-order equation for the normal velocity and a second-order equation for the normal component of vorticity. Streamwise and spanwise velocity components are recovered from the incompressibility condition. If we define the Reynolds number as $Re = UH/\nu$, the convective term as $\hat{v}_i = [\boldsymbol{v} \times \boldsymbol{\omega}]_i$ and the normal component of vorticity as $\psi = \partial v_x/\partial y - \partial v_y/\partial x$, (1) takes the form

$$\frac{\partial}{\partial t}\nabla^2 v_z = f_v + \frac{1}{Re}\nabla^4 v_z, \tag{7}$$

$$\frac{\partial}{\partial t}\psi = f_\psi + \frac{1}{Re}\nabla^2 \psi, \tag{8}$$

where $$f_v = \Delta \hat{v}_z - \frac{\partial}{\partial z}\mathrm{div}(\hat{v}) \quad \text{and} \quad f_\psi = \mathrm{rot}_z(\hat{v}).$$

Here the incompressibility condition has already been taken into account.

The boundary conditions at the wall are

$$\psi|_{wall} = v_z|_{wall} = \frac{\partial}{\partial z} v_z|_{wall} = 0. \tag{9}$$

The boundary conditions at the free surface are more complicated. The conditions on the tangential components of stresses (see (4)) can be expressed straightforwardly in the form

$$\frac{\partial}{\partial z}\psi|_{fs} = Re\left(\frac{\partial}{\partial x}\tau_{yz}|_{ext} - \frac{\partial}{\partial y}\tau_{xz}|_{ext}\right) = W_{rot}, \tag{10}$$

$$\frac{\partial^2 v_z}{\partial z^2}|_{fs} - \nabla_\alpha^2 v_z|_{fs} = -Re\left(\frac{\partial}{\partial x}\tau_{xz}|_{ext} + \frac{\partial}{\partial y}\tau_{yz}|_{ext}\right) = W_{div} \tag{11}$$

where the subscript α again indicates horizontal components. The third boundary condition on v_z is obtained through the relation for pressure at the surface. In our numerical scheme, the pressure computation is not required for time advancement.

Should data on pressure be needed for turbulent statistics, it can be calculated by two different but essentially equivalent ways. One can either use the equation for the normal component of velocity v_z with the wall pressure values determined from an equation for $\partial_\alpha v_\alpha$, or one can use the equation for $\partial_\alpha v_\alpha$ with the pressure corresponding to zero wavenumbers determined from the v_z-equation. Therefore, it is convenient to impose the pressure boundary condition in the following form:

$$\left.\begin{aligned} \frac{\partial}{\partial t}\partial_z v_z &= \Delta_\alpha \pi - \partial_\alpha \hat{v}_\alpha + \frac{1}{Re}\Delta(\partial_z v_z), \\ \pi &= gh - \sigma_* \Delta h + \frac{2}{Re}\partial_z v_z + \frac{v^2}{2} - p_{ext}. \end{aligned}\right\} \tag{12}$$

Here the equation for $\partial v_z/\partial z$ is obtained from the equation for $\partial_\alpha v_\alpha$.

Time stepping is carried with a semi-implicit scheme involving a Crank–Nicolson scheme for the viscous terms and an Adams–Bashforth scheme for the nonlinear terms. For the time advancement of surface height we use a Crank–Nicolson scheme for the normal velocity component and an Adams–Bashforth scheme for the convective term (Canuto *et al.* 1987). Equation (8) then reduces to

$$\left(1 - \frac{\delta t}{2Re}\nabla^2\right)\psi^{n+1} = \tfrac{1}{2}\delta t(3f_\psi^n - f_\psi^{n-1}) + \left(1 + \frac{\delta t}{2Re}\nabla^2\right)\psi^n, \tag{13}$$

with the boundary conditions (9), (10). Equation (13) is solved by the Chebyshev-tau method for each horizontal Fourier component of the vorticity field.

The fourth-order equation (7) is solved by splitting it into two second-order equations

$$\left.\begin{aligned} \left(1 - \frac{\delta t}{2Re}\nabla^2\right)\phi^{n+1} &= \tfrac{1}{2}\delta t(3f_v^n - f_v^{n-1}) + \left(1 + \frac{\delta t}{2Re}\nabla^2\right)\phi^n, \\ \nabla^2 v_z^{n+1} &= \phi^{n+1}, \end{aligned}\right\} \tag{14}$$

with the boundary conditions (9), (11), and the pressure boundary condition (12) which has the following form:

$$\partial_z v_z^{n+1} - \partial_z v_z^n = \frac{\delta t}{Re}\partial_z^3 v_z^{n+1/2} + \frac{3\delta t}{Re}\nabla_\alpha^2 v_z^{n+1/2} + \delta t\,\nabla_\alpha^2(g_* h^{n+1/2} - p_{ext}) + \tfrac{3}{2}\eta^n - \tfrac{1}{2}\eta^{n-1}. \tag{15}$$

Here

$$v_z^{n+1/2} = \tfrac{1}{2}(v_z^{n+1} + v_z^n), \quad h^{n+1/2} = \tfrac{1}{2}(h^{n+1} + h^n), \quad g_* = g + \sigma_*(k_x^2 + k_y^2),$$
$$\eta = \delta t(\partial_\alpha \hat{v}_\alpha - \nabla_\alpha^2 \tfrac{1}{2}v^2).$$

The time advancement scheme for surface height is

$$\left.\begin{aligned} h^{n+1} - h^n &= \tfrac{1}{2}\delta t(v_z^{n+1} + v_z^n) - \tfrac{1}{2}\delta t(3f_h^n - f_h^{n-1}), \\ f_h &= \frac{\partial}{\partial x_\alpha}(v_\alpha h(x_\alpha)). \end{aligned}\right\} \tag{16}$$

The system of coupled equations (14), (16) and (9), (11), (15) is solved by the Chebyshev-tau method, in which the four boundary conditions are satisfied by means of a Green function technique. This system requires three Green functions G_i. The first two of them solve the equations

$$\left(1 - \frac{\delta t}{2Re}\nabla^2\right)\hat{G}_{1,2} = 0, \quad \nabla^2 G_{1,2} = \hat{G}_{1,2},$$

with the boundary conditions

$$\Delta G_1|_{fs} = G_1|_{fs} = G_1|_{wall} = 0; \quad \Delta G_1|_{wall} = 1;$$

and

$$\Delta G_2|_{wall} = G_2|_{wall} = 0; \quad G_2|_{fs} = 1; \quad \frac{\partial^2 G_2}{\partial z^2}|_{fs} = -k^2 G_2|_{fs}.$$

In order to take into account the 'tau correction', i.e. numerical errors due to the finite number of retained Chebyshev polynomials, it is necessary to introduce a third Green function G_3 which satisfies the equation

$$\Delta G_3 = 0,$$

with the boundary condition

$$G_3|_{wall} = 0; \quad G_3|_{fs} = 1.$$

The third Green function G_3 is used to satisfy equations at the boundary points and the boundary conditions at the same time.

To avoid aliasing errors involved in computing the nonlinear terms pseudo-spectrally, the usual $\frac{2}{3}$ dealiasing procedure is used.

The computations reported here were performed on a 32 Intel iPSC/860 Hypercube. Parallelization of the algorithm is straightforward. The only part of the code that involves nodal communication is the Fourier transform, which is implemented by means of global asynchronous cross-processor transposition (Jackson, She & Orszag 1991). Typical performance of this code on 32 nodes is 5.6 s per time step for 128^3 resolution and 1.4 s for the $64 \times 64 \times 128$ resolution.

The accuracy of the numerical code was examined in two different ways. First we implemented the numerical scheme for closed channel flow and analysed the time evolution of small-amplitude Orr–Sommerfeld modes. In all the tests performed both linear decay and growth rates were predicted with errors of less than 0.01 %. In the second set of tests, we analysed the decay in time of an infinitesimally small wave with given wavenumber k at the free surface. We measured the frequency $\Omega(k)$ and the decay rate $\Gamma(k)$ of the wave and compared them with the theoretical prediction for small-amplitude deep-water waves (Landau & Lifshitz 1987):

$$\Omega(k) = (gk + \sigma_* k^3)^{1/2}; \quad \Gamma(k) = 2\nu k^2. \tag{17}$$

Equation (17) is valid when $\Gamma \ll \Omega$, which is always the case for our range of parameters. It was shown that the frequency $\Omega(k)$ is reproduced by the numerical scheme very accurately (usually in the range of 0.1–0.01 %), provided the time step δt is small enough $\Omega(k)\,\delta t \leqslant 0.2$. Our numerical time advancement scheme has second-order accuracy in time. Since $\Gamma \ll \Omega$ it is necessary to decrease δt even further if we want to obtain the correct value for the decay rate of waves. It may be shown that significant numerical dissipation may be avoided if $\delta t \Omega(k) \leqslant (\Gamma(k)/\Omega(k))^{1/2} \approx (l_v\, k)^{3/4}$. Under this restriction, which is generally not burdensome, we obtained a decay rate that differs from the theoretical one by only 0.1 %. In all our runs, we chose the time step to be small enough to correctly reproduce the dynamics of the surface waves.

4. Wave spectra and turbulence statistics

We consider a channel with depth $H = 2$ and horizontal dimensions $L = \pi$ with periodic boundary conditions imposed in the (x, y)-plane. Most of our calculations were performed with 64×64 resolution in the horizontal plane and 129 grid points in

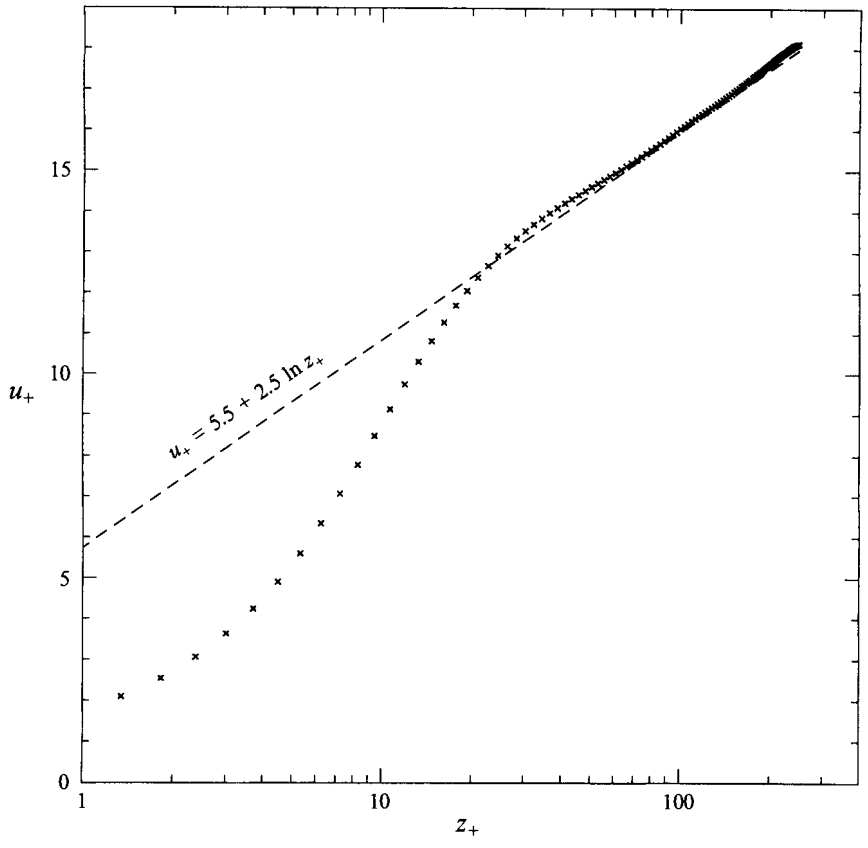

FIGURE 1. Mean-velocity profile: $z_+ = 0$ corresponds to the rigid wall; the dashed line is the law of the wall $u_+ = 5.5 + 2.5 \ln z_+$; $U_{max}/u_* = 18.6$, $U_{max}/U_m = 1.148$.

the normal direction. The emphasis of the present work is the assessment of the feasibility of our approach to compute free-surface flows based on linearization of boundary conditions, and, in particular, on the assessment of general capabilities of the numerical scheme. Therefore, we chose a relatively low resolution in order to be able to carry out more experiments and to cover a broader range of parameters. Several runs, however, were performed with 128^3 resolution, and the results did not differ significantly from the lower-resolution case.

We consider an experimental setup where turbulence is generated through an externally imposed pressure gradient in the x-direction which supplies the centreline mean velocity U. The initial velocity fields were obtained from the standard Orr–Sommerfeld instability modes for channel flow. The flux in the x-direction, i.e. the bulk mean velocity

$$U_m = \frac{1}{2}\int_{-1}^{1} \langle v_x \rangle \, \mathrm{d}z = \tfrac{2}{3},$$

was fixed by adjusting the mean pressure gradient. The viscosity is chosen to be $\nu = 1/3000$ and the maximum mean velocity $U_{max} \approx 0.765$. The Reynolds number defined through the maximum mean velocity is $Re \approx 4560$. The wall-shear velocity is

$$u_* = (\tau_{wall}/\rho)^{1/2} = (\nu \, \partial u_x/\partial z|_{wall})^{1/2} \approx 0.041$$

so that $Re_* = (u_* H)/\nu \approx 250$.

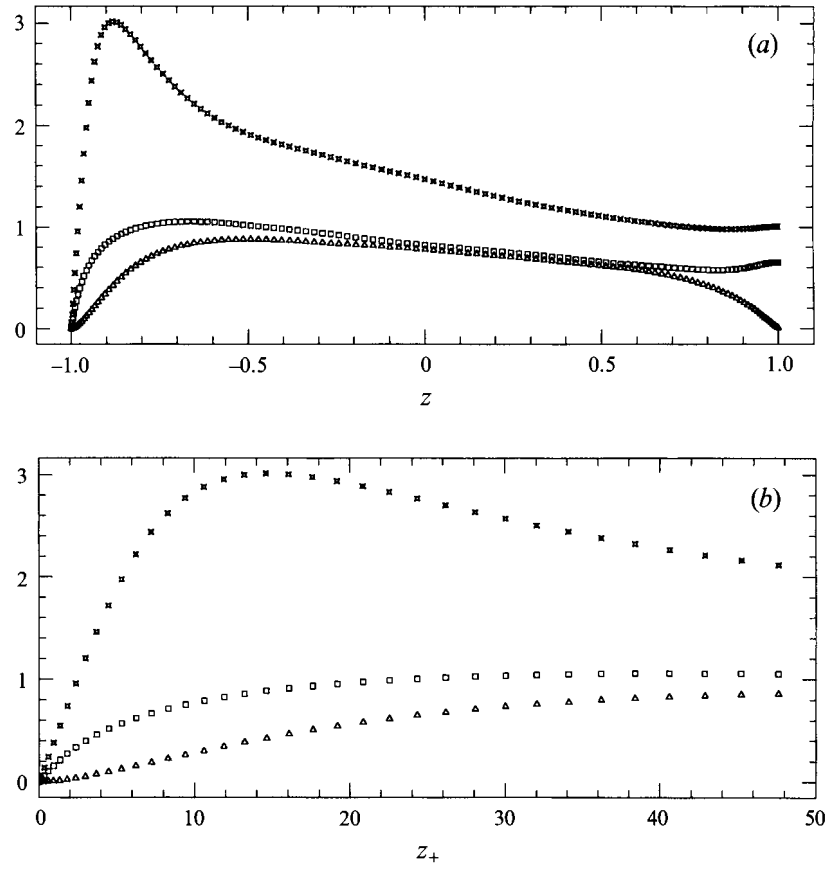

FIGURE 2. Root-mean-square velocity fluctuations normalized by the wall shear velocity: ∖ ×, v_x^{rms}, □, v_y^{rms}; △, v_z^{rms}. (*a*) Global coordinates; (*b*) wall coordinates.

Under these conditions, the Kolmogorov dissipation wavenumber estimated via the energy dissipation rate at the centreline, $\mathscr{E} \approx 5 \times 10^{-5}$ is $k_d = (\mathscr{E}/\nu^3)^{1/4} \approx 35$ and is smaller than the maximum wavenumber in the (x, y)-plane. This means that turbulence in the bulk of the channel and near the rigid wall is well resolved. We believe that the near-free-surface region is also resolved properly. Indeed, the Froude number F_i in our runs varied from 0.1 to 0.6, and the corresponding boundary layer was thick enough to contain several Chebyshev collocation points (although l_v is less than the Kolmogorov dissipation scale). Both criteria (5) and (6) hold in this case and the linearization of the boundary conditions is well based.

4.1. *Channel flow turbulence statistics*

The mean velocity profile is shown in figure 1, where the velocity is normalized by the wall-shear velocity u_* and the distance from the rigid wall z_+ is measured in wall units $z_+ = zu_*/\nu$. As expected the mean velocity profile obeys the law of the wall $u_+ = 2.5 \ln z_+ + 5.5$ starting from approximately $z_+ = 30$. Typically, the mean velocity is slightly larger than one would expect from the law of the wall just near the free surface, in accordance with the data of Nezu & Rodi (1986). Such deviations are likely to result from the effects of the free surface. The data plotted in figure 1 correspond to a typical run with Froude number $F_i \approx 0.55$.

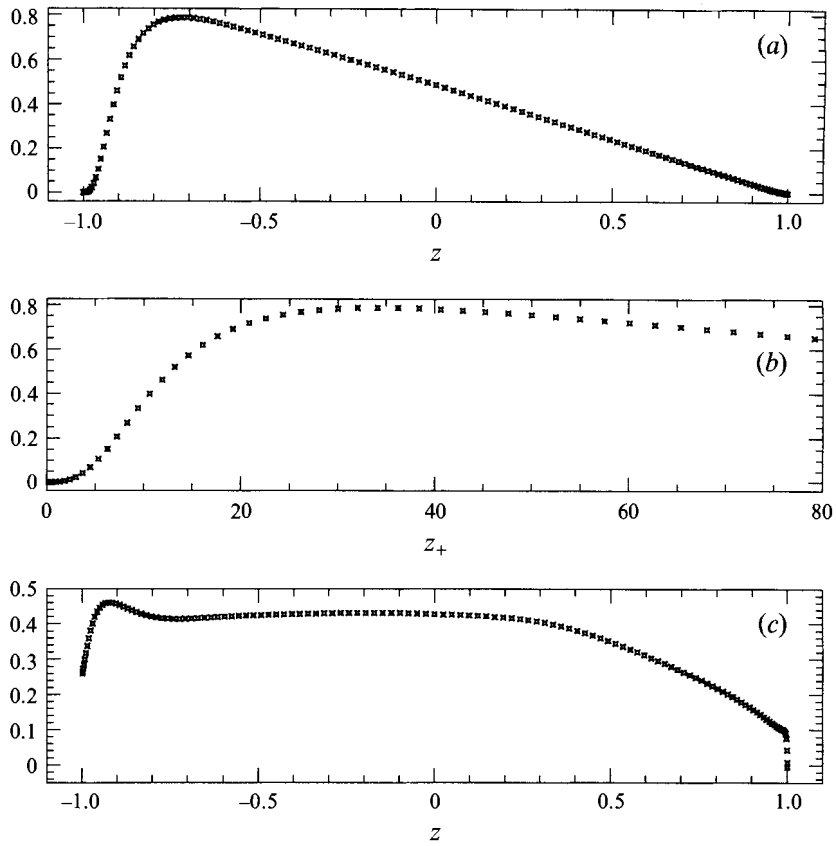

FIGURE 3. Reynolds stress $-\langle v_x v_z \rangle$: (*a*) global coordinates; (*b*) wall coordinates. (*c*) Correlation coefficient $-\langle v_x v_z \rangle / v_x^{rms} v_z^{rms}$ in global coordinates.

Turbulence intensities and Reynolds shear stress normalized by the wall-shear velocity are shown in figures 2 and 3, respectively. The data on r.m.s. vorticity are shown in figure 4. Near the rigid wall and close to the centreline, the profiles are in good agreement with the DNS data on rigid-wall channel flow (Kim *et al.* 1987) and in reasonable agreement with experimental data (Kreplin & Eckelmann 1979). For example, the intensity of streamwise turbulent fluctuations peaks at $z_+ \approx 13$. We have compared our measurements for the skin friction coefficient $C_f = \tau_{wall}/\frac{1}{2}U_m^2$ with the experimental correlations proposed by Dean (1978). The friction coefficient in our case is found to be $C_f \approx 7.6 \times 10^{-3}$, which agrees well with Dean's formula $C_f \approx 0.073 Re_m^{-0.25} \approx 7.7 \times 10^{-3}$ where $Re_m = 2HU_m/\nu \approx 8000$. The ratio U_{max}/U_m is 1.148, also in a good agreement with Dean's data, $U_{max}/U_m = 1.28 Re_m^{-0.0116} = 1.153$. The comparison with available data on turbulence intensities in open-channel flow (Nezu & Rodi 1986) also shows good agreement. The streamwise r.m.s. velocity at the free surface in wall units is roughly 1 in our study and 0.8–1.2 in the experiments, and the spanwise r.m.s. velocity is roughly 0.7 and 0.65, respectively.

It should be mentioned that within the feasible range of Froude numbers (5), typical mean flow profiles do not change significantly with the flow Froude number. Turbulence intensities and r.m.s. vorticity data are also weakly sensitive to the Froude number. We may conclude that for small Froude numbers it is reasonable to consider even the limiting case $F_i = 0$. Such flow in which the gravitation constant g is infinite

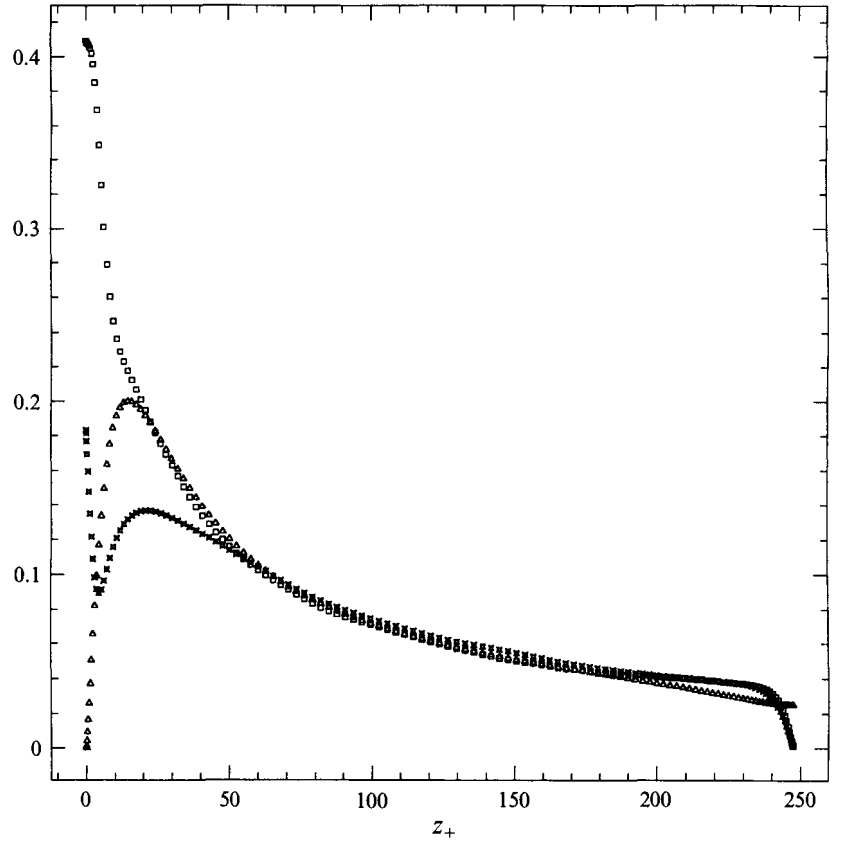

FIGURE 4. Root-mean-square vorticity fluctuations normalized by the mean shear: ×, $\omega_x \nu/u_*^2$; □, $\omega_y \nu/u_*^2$; △, $\omega_z \nu/u_*^2$ in wall coordinates.

can be visualized as corresponding to a half-channel flow with two rigid walls, where inviscid no-stress boundary conditions are imposed at the wall corresponding to the 'free surface' (Hunt & Graham 1978). The presence of such a no-stress wall is the dominant effect at small Froude numbers. In this sense, the free surface responds nearly linearly to the bulk turbulence and does not lead to significant changes in the fluid flow near the free surface compared with the case $F_i = 0$. The dependencies on the flow Froude number are only significant in the near-free-surface region of size $l_w = (2\nu/\Omega_k)^{1/2}$, where Ω_h is some characteristic frequency of turbulence at the free surface. These effects are discussed further in the next Section.

The most important influence of the free surface is that the fluid motion near the free surface is quasi-two-dimensional. The fluctuations of the velocity normal to the surface are substantially smaller than the ones in horizontal directions. The only component of vorticity that is large near the free surface is that normal to the free surface. We may expect that the most important excitations of the free surface come from vortex tubes attached to the free surface at one end, produced by small-scale eddies of nearly two-dimensional turbulence. In this case, an inverse energy cascade may take place that may facilitate the formation of large vortex tubes near the free surface.

Using data on the Reynolds stress and mean velocities, it is possible to obtain distributions of eddy viscosity in open-channel flow. A typical profile of eddy viscosity is plotted in figure 5 at $F_i = 0.55$. Such data may be useful for modelling free-surface

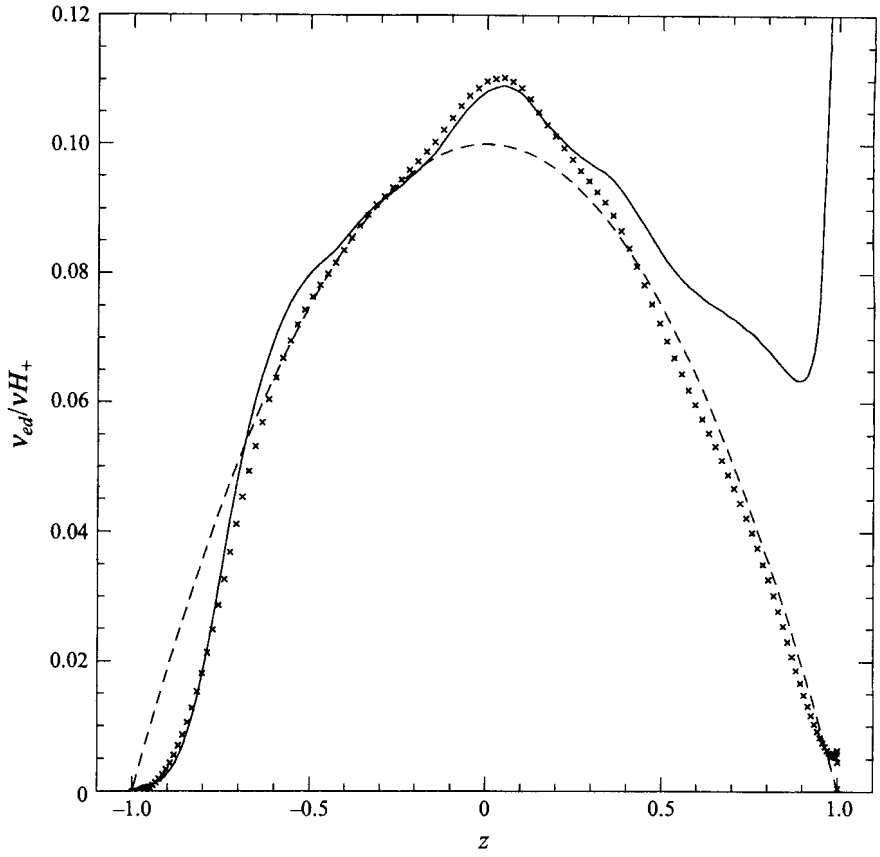

FIGURE 5. Distribution of eddy viscosity $\nu_{eddy}/\nu H_+$ in open-channel flow: ×, measurements; ---, (18); ——, (19) model.

phenomena. Although detailed discussion of this problem is left for a future paper, some preliminary remarks are appropriate here.

First, we compared our data with the empirical formula

$$\frac{\nu_{eddy}}{\nu H_+} = 0.4\frac{z}{H}\left(1-\frac{z}{H}\right). \tag{18}$$

A comparison of (18) with experimental data for open channel flow was made by Ueda *et al.* (1977). Equation (18) implies that the law of the wall is valid throughout the channel, which is certainly not true, at least near the rigid wall. From figure 5, we see that the measured distribution is rather well described by (18) near the free surface.

We have also tried several heuristic formulae which relate eddy viscosity to the turbulent kinetic energy K and the energy dissipation rate $\mathscr{E}$. Recent developments in renormalization group turbulence modelling suggest that the mean rate-of-strain dependence of eddy viscosity is also important (Yakhot *et al.* 1992). The best fit to the present data was found to be given by the following expression:

$$\nu_{eddy} = C_\mu \frac{K^2}{\mathscr{E}} \frac{2}{1+(\eta/a)^2}, \tag{19}$$

where

$$\eta = \frac{\mathrm{d}u_x}{\mathrm{d}z}\frac{K}{\mathscr{E}}.$$

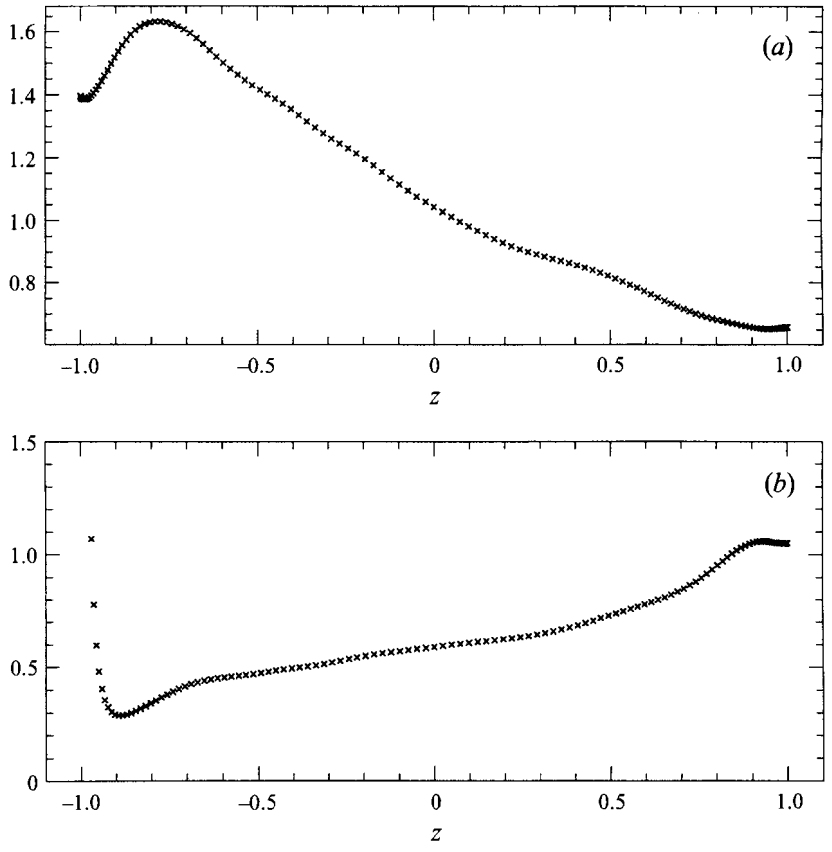

FIGURE 6. (*a*) Root-mean-square pressure fluctuations normalized by the wall shear velocity p_{rms}/u_*^2; (*b*) ratio of root-mean-square pressure fluctuations to the mean kinetic energy.

Using turbulent characteristics K and $\mathscr{E}$ measured from the simulations, we find that the best choice of numerical constants is $C_\mu = 0.09, a = 3.0$. The dimensionless parameter η is the ratio of turbulent to mean strain time scales. Near the rigid wall η is large (≈ 25); in the log-layer of the channel η is approximately constant (between 3 and 4); near the free surface η approaches zero. As the results plotted in figure 5 suggest, the interpolation formula (19) holds rather well near the rigid wall. Close to the free surface, the eddy viscosity given by (19) differs significantly from the measured data, owing to the decrease of energy dissipation rate caused by the zero-stress boundary conditions. This fact implies that the standard K–$\mathscr{E}$ models should be significantly modified near the free surface.

4.2. *Near-free-surface behaviour*

We find that the viscous term in the boundary condition (12) is numerically small and $p_{rms} \approx g h_{rms}$, where $h_{rms} = \langle h^2 \rangle^{1/2}$ is the r.m.s. surface height. On the other hand, the r.m.s. pressure at the free surface $p_{rms} \approx \frac{1}{2}\langle v_i^2 \rangle$ is approximately independent of g (see figure 6). Therefore, the following approximate relation is well satisfied:

$$h_{rms} \approx K_{fs}/g, \tag{20}$$

where K_{fs} is the mean kinetic energy at the surface.

Another observation is that the root-mean-square fluctuations of the streamwise and spanwise velocity components, as well as the normal component of vorticity, are

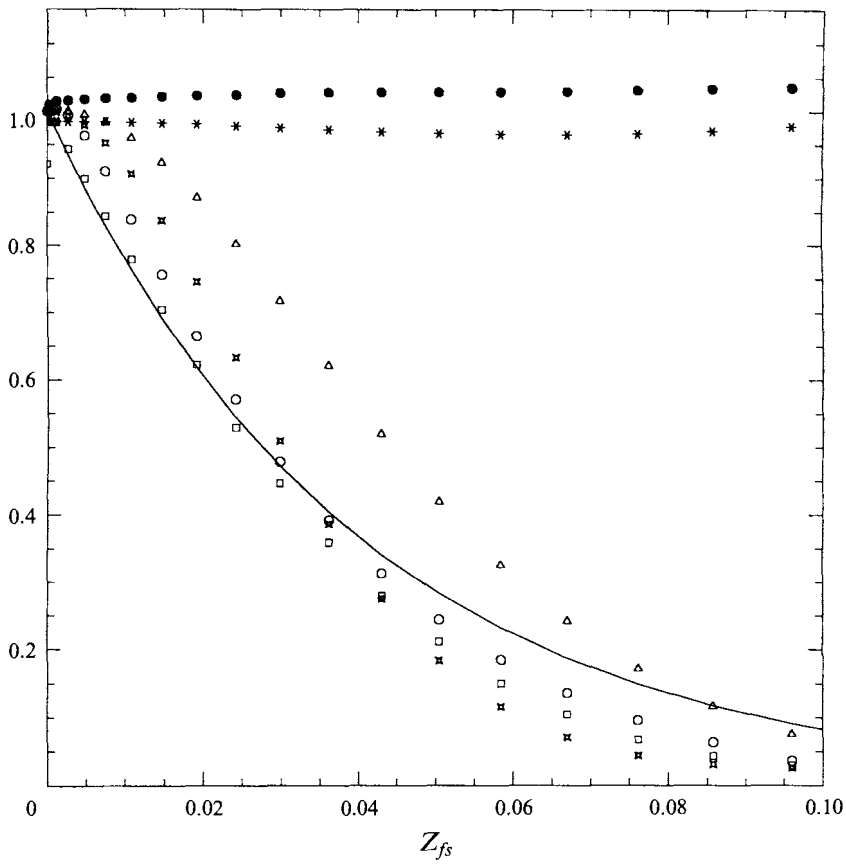

FIGURE 7. Near-free-surface behaviour of flow characteristics. The limiting operator $\hat{\mathscr{F}}$ is applied to: ×, $\mathscr{E}$; △, $\langle \mathrm{d}(v_x v_z)/\mathrm{d}z \rangle$; □, $\langle \mathrm{d}v_x/\mathrm{d}z \rangle$; ○, $\omega_{x,y}^{rms}$. The ratios $K(z_{fs})/K(0)$ and $\omega_z^{rms}(z_{fs})/\omega_z^{rms}(0)$ are shown by * and ●, respectively. The solid line is $\mathrm{e}^{-z_{fs}/\lambda}$ with $\lambda \approx 0.08H$. z_{fs} is the distance from the free surface.

practically independent of g, whereas $v_z|_{rms} \sim 1/g$. The r.m.s. values of streamwise and spanwise components of vorticity are also inversely proportional to g. The scaling of u_z with g and (20) suggest that there exists a characteristic frequency of surface height fluctuations $\Omega_h|_{rms} \approx v_z|_{rms}/h_{rms}$ which is approximately constant in the range of Froude numbers considered. This frequency relates to the characteristic turnover times of the largest turbulent eddies. Within the viscous sublayer, the turbulent kinetic energy K was observed to be practically independent of the distance from the free surface. Therefore, the Neumann boundary condition $\partial K/\partial z = 0$ seems to be relevant for modelling free-surface phenomena.

Most of the averaged quantities or their derivatives vary smoothly in the middle of the channel but vary nearly exponentially near the free surface. To analyse their behaviour, it is convenient to define an operator $\hat{\mathscr{F}}$ of the following form:

$$\hat{\mathscr{F}}(f(z_{fs})) = \frac{f(z_{fs}) - f(\infty)}{f(0) - f(\infty)}. \tag{21}$$

The operator $\hat{\mathscr{F}}$ acts on functions $f(z_{fs})$, where z_{fs} designates the distance from free surface. According to the definition $\hat{\mathscr{F}}(f(0)) = 1$ for any f. For functions which fall off exponentially away from the free surface, $\hat{\mathscr{F}}(f(z_{fs})) \approx \exp(-z_{fs}/\lambda)$. In figure 7, we show the near-free-surface behaviour of different flow characteristics analysed by

means of the limiting operator $\hat{\mathscr{F}}$. Plotted in figure 7 are the mean rate of strain $\langle \mathrm{d}v_x/\mathrm{d}z \rangle$, the energy dissipation rate $\mathscr{E}$, the horizontal components of r.m.s. vorticity $\omega_{x,y}^{rms}$, as well as the z-derivatives of the Reynolds stress $\langle \mathrm{d}(v_x v_z)/\mathrm{d}z \rangle$. Most of these characteristics change exponentially near the free surface as $\sim C_1 - C_2 \exp(-z_{fs}/\lambda)$ with approximately the same exponent $\lambda \approx 0.08H$. If we identify λ with a depth of some skin layer, a characteristic excitation frequency at the free surface can be estimated as $\Omega_0 \approx 2\nu/\lambda^2$. In our setup, such an estimation gives $\Omega_0 \approx 0.42$. It is shown later that this frequency nearly matches the directly measured characteristic frequency of surface wave motion.

As may also be seen from figure 7, the ratio of the turbulent kinetic energy $K(z_{fs})/K(0)$ and the ratio of r.m.s. normal vorticity fluctuations $\omega_z^{rms}(z_{fs})/\omega_z^{rms}(0)$ are approximately constant.

4.3. *Surface wave spectra*

To begin, we analysed the dispersion relation of surface waves. Since the boundary conditions are linearized, we expect the dispersion relation to be given by (17). Let us define two correlation functions of some variable $q(x, t)$:

$$U_q(k) = \int \langle q(x,t)\, q(0,t) \rangle \exp(\mathrm{i}kx)\, \mathrm{d}x, \tag{22}$$

$$S_q(k, \Omega) = \int \langle q(x,t)\, q(0,0) \rangle \exp(\mathrm{i}kx + \mathrm{i}\Omega t)\, \mathrm{d}x\, \mathrm{d}t \tag{23}$$

so that $U_q = \int (\mathrm{d}\Omega/2\pi) S_q$. Here k stands for the wave vector in the horizontal plane and all quantities are evaluated at the free surface. The correlation functions U_q are directly measured in our numerical experiments, whereas the evaluation of the functions S_q requires rather expensive time averaging. In our case, a linearized version of (3) yields

$$S_h(k, \Omega) = \frac{1}{|\Omega|^2} S_{v_z}(k, \Omega), \tag{24}$$

and for the equal-time spectral densities:

$$U_h(k) = \int \frac{1}{|\Omega|^2} S_{u_z}(k, \Omega) \frac{\mathrm{d}\Omega}{2\pi}. \tag{25}$$

In the low-k region ($k \ll 1/l_w$), the singularities of the correlation function S_h are dominated by the oscillatory part of dispersion relation. Using (17), we obtain

$$U_h(k) = C(k)\, U_{v_z}(k), \quad C(k) = \frac{1}{|\Omega|^2(k)}. \tag{26}$$

At this point, it is important to mention that the spectra U_h and U_z themselves may be far from those corresponding to the linear surface waves problem. Also the relation (26) does not require potentiality of the surface flow. The only assumption that was used in the derivation of (26) is that the Green function for the equation for normal velocity has a pole at the characteristic frequency given by (17), whereas the dissipative term in the dispersion relation is negligible. Such an assumption may become invalid owing to the effects of turbulence. Also, the effects of the mean flow in our case can, in principle, complicate the dispersion relation structure. The ratio

$$\Omega_h(k) = \left(\frac{U_{v_z}(k)}{U_h(k)} \right)^{1/2} \tag{27}$$

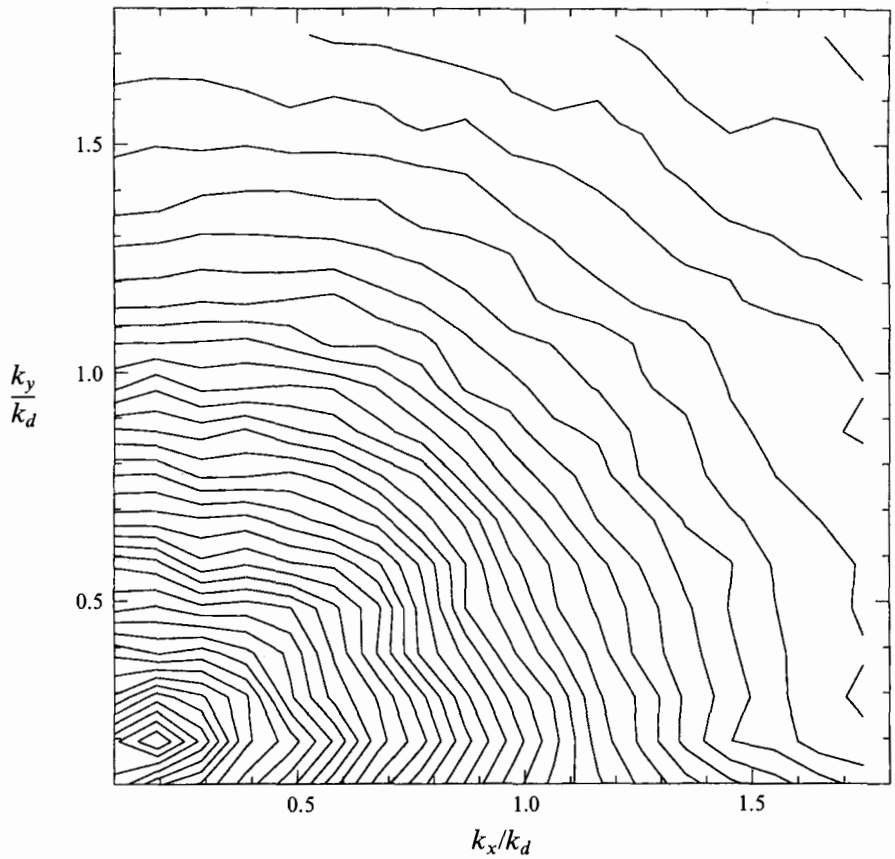

FIGURE 8. Two-dimensional spectrum of characteristic surface frequencies. Lines of constant $\log(\Omega_h(k))$ as the function of k_x/k_d, k_y/k_d are shown.

may be called a characteristic frequency of surface height excitations at wavenumber k. Measurements of the spectra (27) can serve as a diagnostic tool to analyse the properties of near-free-surface turbulence.

In figure 8, we show the two-dimensional spectrum of the logarithm of characteristic wave frequencies. The shape of the spectrum is practically isotropic in the (k_x, k_y)-plane so that the dispersion relation can be well represented by the 'one-dimensional' spectrum shown in figure 9. The one-dimensional spectrum is obtained from the isotropic two-dimensional spectrum by summing all the $U_q(k)$ with k on a circle of a given radius $|k|$. When $k/k_d \geqslant 1$, the measured dependence $\Omega_h(k)$ is well described by (17). At smaller wavenumbers, the function $\Omega_h(k)$ deviates significantly from (17) and reaches an approximately constant value Ω_0. This behaviour of the characteristic frequency reflects the influence of 'bottom-generated' turbulence upon the surface wave behaviour. The wave spectra in the low-k region $k/k_d \leqslant 1$ are forced by the turbulence. The frequency Ω_0 depends on the flow Reynolds number only and characterizes the frequency of the attached vortex tubes. In the turbulence dissipation range, nonlinear effects are small and surface waves can be considered as freely evolving. It should be noted that the numerical value of the limiting frequency $\Omega_0 = \Omega(k \to 0) \approx 0.5$ is close to the estimate obtained in §4.2.

The spectra of surface height $h(k)$, and velocity components $v_{x,y}(k), v_z(k)$ are also isotropic in wavenumber space. The one-dimensional spectra are plotted in figure 10.

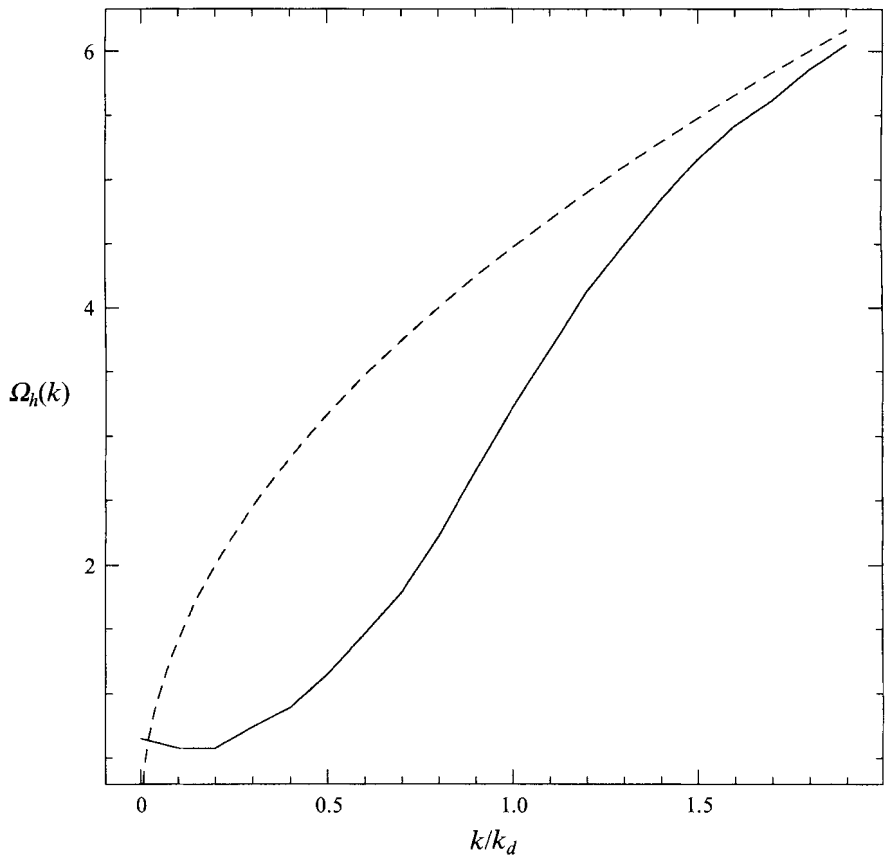

FIGURE 9. Spectra of characteristic surface frequencies $\Omega_h(k)$ as a function of k/k_d for $F_i \approx 0.55$ (solid line). The dashed line is $\Omega(k) = (gk)^{1/2}$.

The spectral behaviour of the surface correlation function differs significantly from the Phillips' surface wave spectral laws $1/k^3$ (Phillips 1977) or $1/k^{7/2}$ (Phillips 1985). In fact, the spectral index is between one and two. This fact is not very surprising, because we are mostly concerned with spectra of small surface waves forced by the bulk turbulence. Linearization of the free-surface boundary definitely contributes to this discrepancy. Surface waves in our problem play the role of a diagnostic tool that enables us to measure spectral characteristics of bulk turbulence. On the other hand, Phillips' spectrum may be observed in the so-called wave saturation range for waves in the ocean, where nonlinear wave interaction is essential. Our data are in reasonable agreement with the low Froude number data of Brumley & Jirka (1987) where the spectra of free-surface velocity fluctuations were measured for the case of grid-generated turbulence with a grid at the bottom of the tank.

For all Froude numbers that we considered, the characteristic surface frequencies Ω_h were lower than the free-surface frequencies (17). When the gravitational constant g decreases, these frequencies match and resonant excitations of the surface waves occur. This leads to wave breaking phenomena. Unfortunately, in this regime our numerical algorithm breaks down owing to incorrect free-surface boundary conditions.

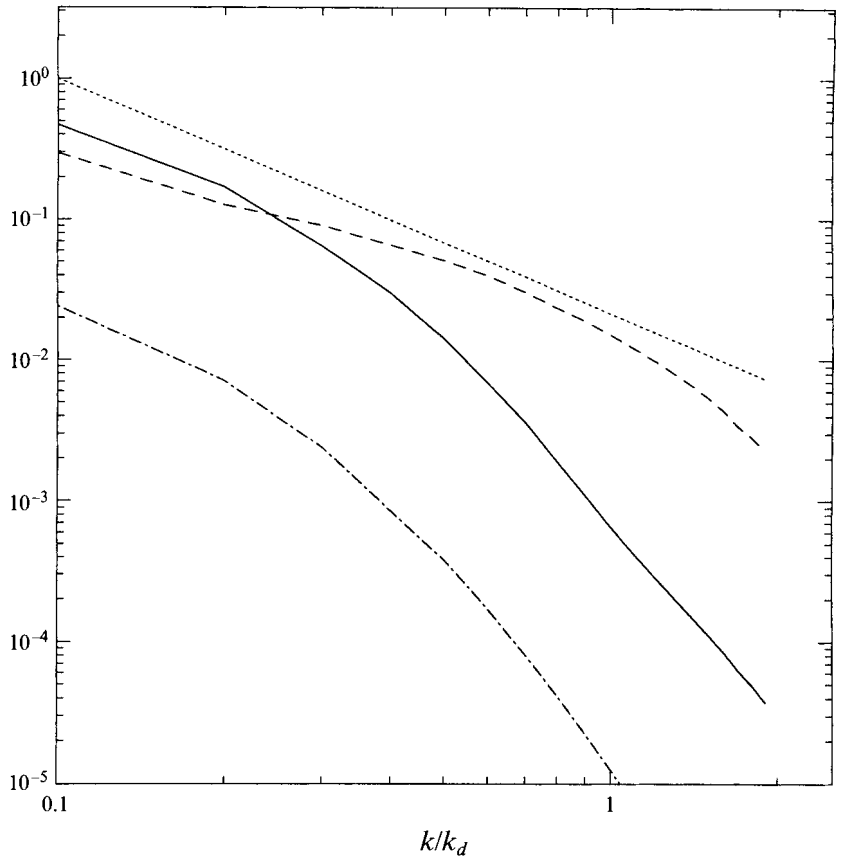

FIGURE 10. One-dimensional spectra of: surface height correlator $U_h(k)/h_{rms}^2$ (——); the normal velocity at the surface correlator $U_{v_z}(k)/\langle v_z^2\rangle|_{fs}$ (– – – –); the tangential velocity at the surface correlator $10^{-1}U_{v_{x,y}}(k)/\langle v_{s,y}^2\rangle|_{fs}$ (—·—·—), all as a function of k/k_d. The dotted line is $1/k^{5/3}$.

4.4. *Externally generated turbulence*

Here we discuss some preliminary results concerning simulation of turbulence generated by external stresses and pressure, as a model of wind-generated surface wave phenomena. So far, we have considered only a few simple cases where the spectra of external stresses are far from those experimentally observed. The generalization of our approach to include external stresses of different shapes and angular dependencies is straightforward.

We have chosen an external stress oscillating in time and taking non-zero values only at the lowest wavenumbers ($k_x = k_y = 2$ in our geometry):

$$A\cos(k_x x + \Omega_f t + \phi_x) + A\cos(k_y y + \Omega_f t + \phi_y). \tag{28}$$

In real open-surface flows, the external stress tensor may contain diagonal components (the pressure p_{ext}) as well as non-diagonal components (the strain τ_{ext}). The external strain can also have divergence-free components W_{rot} and vorticity-free components W_{div}. The corresponding boundary conditions have the form (10), (11).

External perturbations have a finite penetration depth for vorticity components of this perturbation (Landau & Lifshitz 1987):

$$l_w = (2\nu/\Omega_0)^{1/2}. \tag{29}$$

In our study, the characteristic perturbation frequency can be identified with

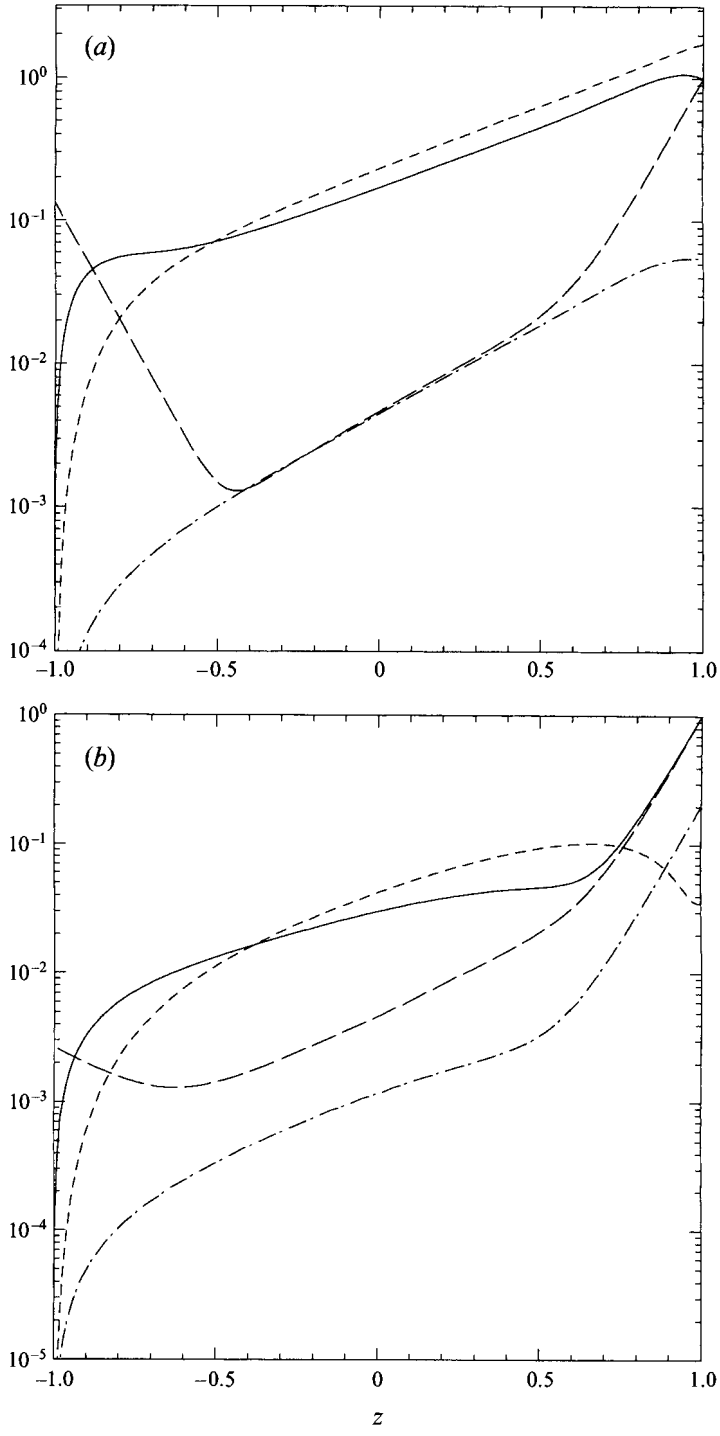

FIGURE 11(*a*,*b*). For caption see facing page.

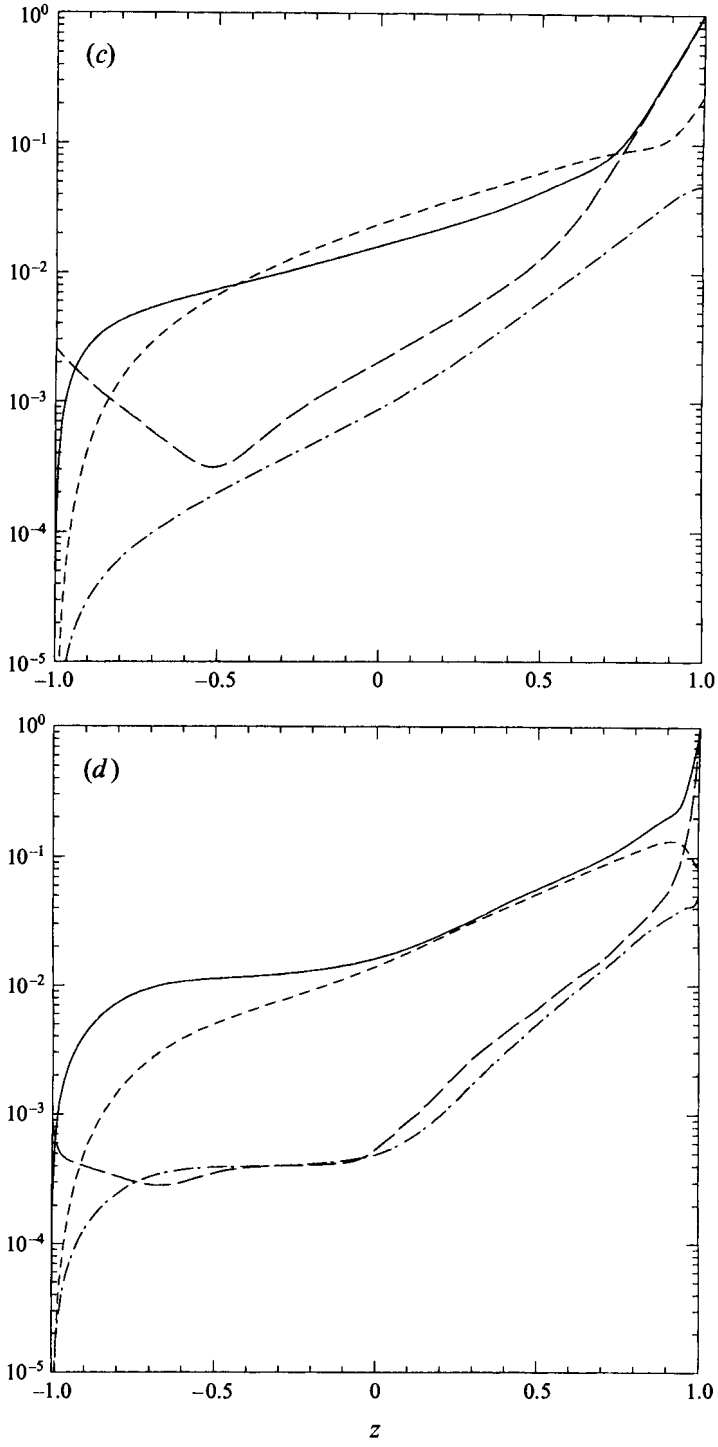

FIGURE 11. Root-mean-square velocity and vorticity fluctuations normalized by their free-surface r.m.s. values of the corresponding horizontal components: ——, tangential velocity; – – –, normal velocity; ———, tangential vorticity; —·—·—, normal vorticity. (*a*) Externally applied pressure; (*b*) divergence-free external stress; (*c*) curl-free external stress; (*d*) $Re_w = 5$.

$\Omega_0 = \min(\Omega_{fs}^{min}, \Omega_f)$, where Ω_{fs}^{min} is the lowest eigenfrequency of the free surface (see (17)). The characteristic velocity at the free surface for sufficiently small Froude numbers is

$$u_* = (\tau_{fs}/\rho)^{1/2}, \tag{30}$$

where τ_{fs} is the stress at the free surface. The Reynolds number in the near-surface region can be defined as

$$Re_w = \min\left(\frac{u_* H}{\nu}, \frac{u_*}{(\nu\Omega_0)^{1/2}}\right). \tag{31}$$

It follows from the definition (31) that when $l_w \leqslant H$, externally generated perturbations do not reach the bottom and H is not the relevant parameter. In all our numerical experiments, the wave amplitude was smaller than the penetration length l_w thus justifying the applicability of the linearized boundary condition.

As the simplest example, consider waves generated only by an oscillating external pressure. The frequency of the external perturbation was chosen so that $Re_w \approx 0.1$ and $l_w/H \approx 0.05$. The calculated mean-squared velocities and vorticities normalized by their free-surface values for corresponding horizontal components are shown in figure 11 (*a*). As may be seen from figure 11 (*a*), both the r.m.s. velocity and vorticity decay away the free surface (at $z = 1$) according to the exponential law $\exp(-\lambda(1-z))$. It was checked that the decay exponent λ for the velocity is equal to the force wavenumber $k_x = k_y = 2$, and the decay exponent for the tangential vorticity component is equal to $\lambda = 1/l_w$, as one would expect on the basis of linear theory (Landau & Lifshitz 1987). It is interesting to note that, near the rigid wall, the tangential vorticity component increases with approximately the same rate as it decays off the free surface.

As the next two examples, we consider generation of waves by an external oscillating strain of the form (28) with $Re_w \approx 1.5$ and $l_w/H \approx 0.05$. In the first case, a divergence-free stress W_{rot} was applied. In the second case, a purely curl-free stress W_{div} is applied. The corresponding profiles of turbulence characteristics are shown in figures 11 (*b*) and 11 (*c*). The near-centreline behaviour of r.m.s. velocities and vorticities is similar to the previous example. The substantial difference is that the free-surface r.m.s. values of the normal velocity component are much smaller than the horizontal ones. The corresponding intensity ratios are approximately 0.33 for the curl-free stress and 0.05 for the divergence-free stress. The explanation is that the externally applied strain mostly transfers energy into the tangential velocity components, creating large vorticity at the free surface. When the stress is divergence-free, the normal vorticity component is much larger than in the case of curl-free stress, thus leading to an effective attenuation of surface waves. It is curious to note that in the case of divergence-free stress, the maximum of the intensity of the normal velocity component is at a depth $\sim l_w$.

In the cases considered above, the Reynolds number Re_w was rather slow and in fact the flow was only marginally turbulent. We have also performed several runs at higher Re_w. Data obtained in a typical run corresponding to $Re_w = 5$ are plotted in figure 11 (*d*). The external stress was composed of a mixture of different components. The shapes of the velocity spectra suggest that the flow with such a seemingly small value of Re_w exhibits behaviour typical of well-developed turbulent flows. As can be seen from figure 11, the profiles of r.m.s. velocity and vorticity in the region far from the surface are similar to those obtained at lower Reynolds numbers (see figure 11 *a–c*). It might be concluded that the specific structure of externally imposed stresses mostly influences the near-free-surface flow pattern, and plays a rather minor role elsewhere.

To have an impression of how the external stress at the free surface influences the mean velocity profile in open-channel flow, computations with an external stress

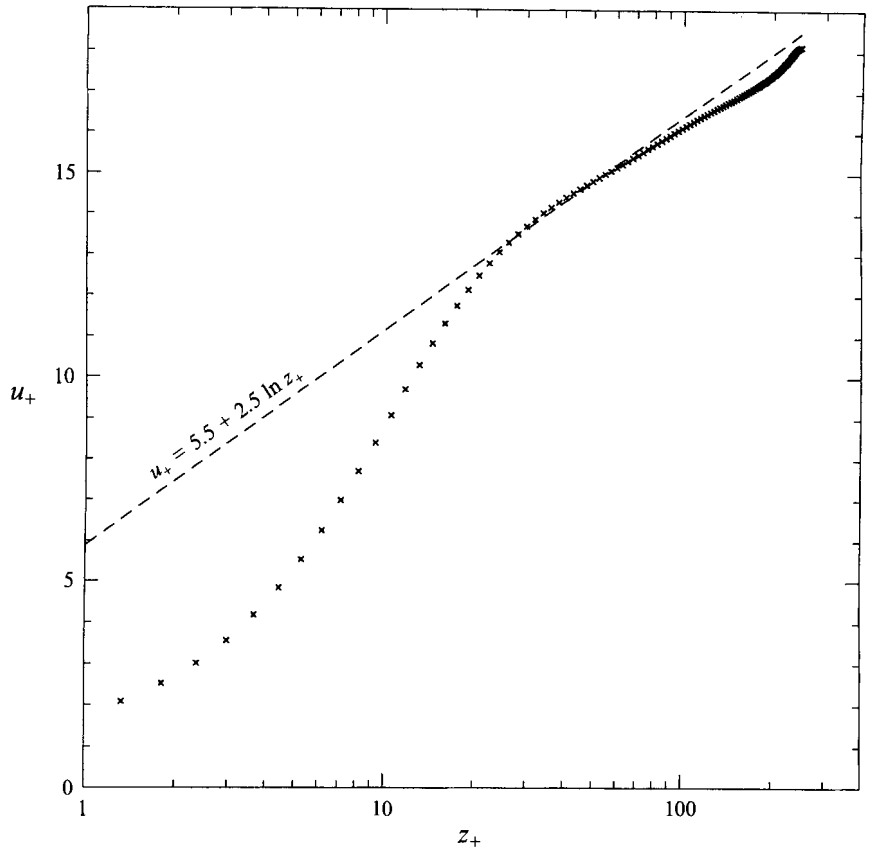

FIGURE 12. Mean-velocity profile; open-channel flow with oscillating external stress at the free surface. The dashed line is the law of the wall $u_+ = 5.5 + 2.5 \ln z_+$.

constant in space and oscillating in time were performed. The oscillation frequency was chosen to be only slightly lower than Ω_{fs}^{min}, and the magnitude of the stress was approximately 20 % of its value at the rigid wall. The mean velocity profile for this case is shown in figure 12. It may be observed that the mean velocity profile is substantially changed near the free surface. Such details of near-free-surface behaviour of mean flow characteristics are treated well by our code and should be studied further.

5. Discussion

The main goal of this work was to test the feasibility of direct numerical simulation of free-surface flows at Reynolds numbers corresponding to state-of-the art simulations of wall-bounded turbulence. Therefore, we have concentrated upon the simplest flows with the simplest experimental configuration. There are additional phenomena which can be incorporated into our computational scheme rather straightforwardly, including transport of passive scalars, thermal stratification in the Boussinesq approximation, and internal waves in the ocean. Our approach can also be extended to study flows in complex geometries with basically the same domain decomposition spectral-element techniques that are now used for wall-bounded flows.

Our first test case, where the turbulence was generated 'from below', i.e. by the shear production of energy at the rigid wall, is relevant to the problem of diagnosing interior

turbulence properties through the observation of the statistics of waves at the surface. The influence of particular mechanisms of energy production upon spectra of the surface height deserve further investigation. The second case where the turbulence is generated by stresses at the surface is relevant to the problem of turbulent mixing in the upper ocean. In future research, it will be interesting to consider more realistic spectra of the externally imposed stresses, i.e. to take into account spatial, angular and temporal variability of the stress. Another possible extension of our approach, which seems to be potentially important for applications in physical oceanography and atmospheric sciences, would be to take into account non-zero viscosity in the adjacent media and thus consider the air–sea interaction. This would provide insight into the mechanisms of wind-generated waves, turbulent spectra within the air surface boundary layer, the phenomena of bursting at the air–sea interface and other problems.

We close by summarizing issues that are left open here. First, we do not have any comprehensive theoretical explanation for the scaling behaviour at large interaction times, an extremely challenging and important question. Next, the Reynolds numbers achievable in our computations are several orders of magnitude below that of real geophysical flows, so that there is a need for different kinds of modelling. We believe that the large-eddy simulation schemes that can be used here should be similar to those used for wall-bounded turbulence. At the same time, the direct simulation results can provide the necessary database for modelling of near-free-surface boundary layers, particularly in K–$\mathscr{E}$ and algebraic model formalisms.

High-resolution simulations of finite-amplitude surface waves interacting with fully developed turbulence are not yet possible. An alternative approach to the simulation of free-surface flows with high-amplitude surface waves is to map the physical domain onto the computational domain $-\frac{1}{2}H < z < \frac{1}{2}H$ and then to apply Chebyshev spectral methods. Any use of a conformal mapping formalism is obviously restricted to the two-dimensional case and thus does not address the real physics. In any case, wave breaking phenomena, which represent the key feature of nonlinear surface waves interaction and are responsible for most of the dissipation within viscous sublayers in real fluids, are unlikely to be captured by mapping techniques. Our formulation of the problem, which neglects nonlinear self-interaction of waves and retains the turbulence, is an effective approach which is self-consistent and feasible for at least one class of interesting problems.

We are grateful to Victor Yakhot for discussions. This work was supported by DARPA, ONR and AFOSR under Contracts N00014-92-J-1796, N00014-90-C-0039, N00014-92-C-0039 and F49620-91-C-0059.

REFERENCES

BRUMLEY, B. H. & JIRKA, G. H. 1987 Near-surface turbulence in a grid-stirred tank. *J. Fluid Mech.* **183**, 235.

CANUTO, C., HUSSAINI, M., QUARTERONI, A. & ZANG, T. 1987 *Spectral Methods in Fluid Dynamics.* Springer.

CELIK, I. & RODI, W. 1984 Simulation of free-surface effects in turbulent channel flows. *Phys. Chem. Hydrodyn.* **5**, 217.

DEAN, R. B. 1978 Reynolds number dependence of skin friction and other bulk flow variables in two-dimensional rectangular duct flow. *Trans. ASME* I: *J. Fluids Engng* **100**, 215.

GIBSON, M. M. & RODI, W. 1989 Simulation of free surface effects on turbulence with a Reynolds stress model. *J. Hydraul. Res.* **27**, 233.

HANDLER, R. A., SWEARINGEN, J. D., SWEAN, T. F. & LEIGHTON, R. I. 1991 Length scales of turbulence near a free surface. *AIAA Paper* 91-1775.

HUNT, J. C. R. & GRAHAM, J. M. R. 1978 Free-stream turbulence near plane boundaries. *J. Fluid Mech.* **84**, 209.

JACKSON, E., SHE, Z. & ORSZAG, S. 1991 A case study in parallel computing: I. Homogeneous turbulence on a hypercube. *J. Sci. Comput.* **6**, 27.

KIM, J., MOIN, P. & MOSER, R. 1987 Turbulence statistics in fully developed channel flow at low Reynolds number. *J. Fluid Mech.* **177**, 133.

KIRKGOZ, M. S. 1989 Turbulent velocity profiles for smooth and rough open channel flow. *J. Hydraul. Engng ASCE* **115**, 1543.

KREPLIN, H. & ECKELMANN, H. 1979 Behavior of the three fluctuating velocity components in the wall region of a turbulent boundary layer. *Phys. Fluids* **22**, 1233.

LANDAU, L. D. & LIFSHITZ, E. M. 1987 *Fluid Mechanics*. Pergamon.

LEIGHTON, R. I., SWEAN, T. F., HANDLER, R. A. & SWEARINGEN, J. D. 1991 Interaction of vorticity with a free surface in turbulent open channel flow. *AIAA Paper* 91-0236.

NEZU, I. & RODI, W. 1986 Open channel flow measurements with a laser Doppler anemometer. *J. Hydraul. Engng ASCE* **112**, 335.

PHILLIPS, O. M. 1977 *The Dynamics of the Upper Ocean*. Cambridge University Press.

PHILLIPS, O. M. 1985 Spectral and statistical properties of the equilibrium range in wind-generated gravity waves. *J. Fluid Mech.* **156**, 505.

SWEAN, T. F., LEIGHTON, R. I., HANDLER, R. A. & SWEARINGEN, J. D. 1991 Turbulence modeling near the free surface in an open channel flow. *AIAA Paper* 91-0613.

UEDA, H., MÖLLER, R., KOMORI, S. & MIZUSHINA, T. 1977 Eddy diffusivity near the free surface of open channel flow. *Intl J. Heat Mass Transfer* **20**, 1127.

YAKHOT, V., ORSZAG, S. A., THANGAM, S., GATSKI, T. B. & SPECIALE, C. G. 1992 Development of turbulence models for shear flows by a double expansion technique. *Phys. Fluids* A **4**, 1510.